Regular Article

Effects of alloying chalcopyrite CuTlSe$_2$ with Na on the electronic structure and thermoelectric coefficients: DFT investigation

K. Djelid[1]**, T. Seddik**[1,a] **, O. Merabiha**[1]**, M. Batouche**[1]**, R. Khenata**[1,b]**, A. Bouhemadou**[2]**, Saleem Ayaz Khan**[3]**,
S. Bin Omran**[4]

[1] Laboratory of Quantum Physics of Matter and Mathematical Modeling (LPQ3M), Mascara University, Mascara, Algeria
[2] Laboratory for Developing New Materials and Their Characterizations, Department of Physics, Faculté of Sciences, University Ferhat Abbas Setif 1, 19000 Sétif, Algeria
[3] New Technologies - Research Center, University of West Bohemia, Univerzitni 8, 306 14 Pilsen, Czech Republic
[4] Department of Physics and Astronomy, College of Science, King Saud University, P.O. Box 2455, Riyadh 11451, Saudi Arabia

Abstract The optimized structural parameters, electronic structure, and thermoelectric coefficients of the chalcopyrite alloys Cu$_{1-x}$Na$_x$TlSe$_2$, with $x = 0.00$, 0.25, and 0.50 were studied through density functional theory calculations. The Wu–Cohen generalized gradient and the Tran–Blaha modified Becke–Johnson approximations have been employed to describe the exchange–correlation potential. Energy band structure analysis reveals that CuTlSe$_2$ is a semi-metal, while Cu$_{0.25}$Na$_{0.75}$TlSe$_2$ and Cu$_{0.50}$Na$_{0.50}$TlSe$_2$ alloys are semiconductors with gaps of approximately 0.17 eV and 0.35 eV, respectively. The total and partial densities of states were calculated and discussed. Examining the charge density, we point out the formation of the Na–Se ionic bond when Cu is replaced by the Na atom, which is responsible for the metal–semiconductor transition in the Cu$_{1-x}$Na$_x$TlSe$_2$ alloys. Moreover, variations of the Seebeck coefficient, electrical conductivity, electronic and lattice thermal conductivity, power factor, and figure of merit of the Cu$_{1-x}$Na$_x$TlSe$_2$ alloys with temperature and chemical potential were explored. The obtained results show that the value of the figure of merit increases when doping CuTlSe$_2$ with sodium to reach 0.46 and 0.87 for p-type Cu$_{0.75}$Na$_{0.25}$TlSe$_2$ and n-type Cu$_{0.50}$Na$_{0.50}$TlSe$_2$, respectively.

1 Introduction

Many research groups are now focusing on the quest for novel materials that can be used for energy conversion applications. Thermoelectric (TE) materials have the ability to convert heat directly into useful electrical energy according to the Seebeck effect and to pump heat according to the Peltier effect. Thus, TE materials have received increasing global attention since the discovery of bismuth telluride Bi$_2$Te$_3$ in 1960 [1], which is the reference thermoelectric material. Many families of materials, such as clathrates [2], skutterudites [3, 4], and Zintl phases [5], have proven to be effective TE materials since this first discovery.

The efficiency of TE materials is governed by a dimensionless physical parameter known as "figure of merit," which is defined as follows: $ZT = \frac{S^2\sigma}{\kappa_e + \kappa_l}$, where σ represents the electrical conductivity, S represents the Seebeck coefficient, κ_e represents the electronic thermal conductivities, κ_L represents the lattice thermal conductivities, and T represents the absolute temperature. The thermoelectric performance of a TE material can be enhanced in different ways such as through convergence of electronic band valleys [6], adding impurities or by creating point defects through alloying [7–9], and making superlattices from thin films [10]. On the other hand, searching for materials having low thermal conductivity, a large Seebeck coefficient and high electrical conductivity present a serious dilemma. This is because these parameters are inversely dependent on the charge carriers.

Here, we report the results of a detailed investigation of the electronic structure and thermoelectric properties of the CuTlSe$_2$ compound, which is a Weyl semimetal material and possess a correlated-electron system [11]. Furthermore, the CuTlSe$_2$ compound belongs to the Cu-based chalcopyrite family, including the CuGaTe$_2$, CuInTe$_2$, CuAlSe$_2$, and CuAlTe$_2$ compounds, which exhibit interesting thermoelectric properties [12–14]. Some researcher groups tried to enhance the thermoelectric performance of chalcopyrite by doping them with different transition metal atoms, such as doping CuFeS$_2$ with Zn, Mn, Co, Ni, and Pd atoms [15, 16], CuInTe$_2$ [17] and CuGaTe$_2$ [18] with Ag element, and CuGaTe$_2$ with Mn atom [19]. Besides, it is reported that the sodium substitution affects the electronic properties and improves the TE character of semiconductors [20] and metallic materials [21]. To the best of our knowledge, to date neither detailed experimental measurements nor theoretical investigations regarding the Na-doped

[a] e-mail: seddik.taib@univ-mascara.dz (corresponding author)
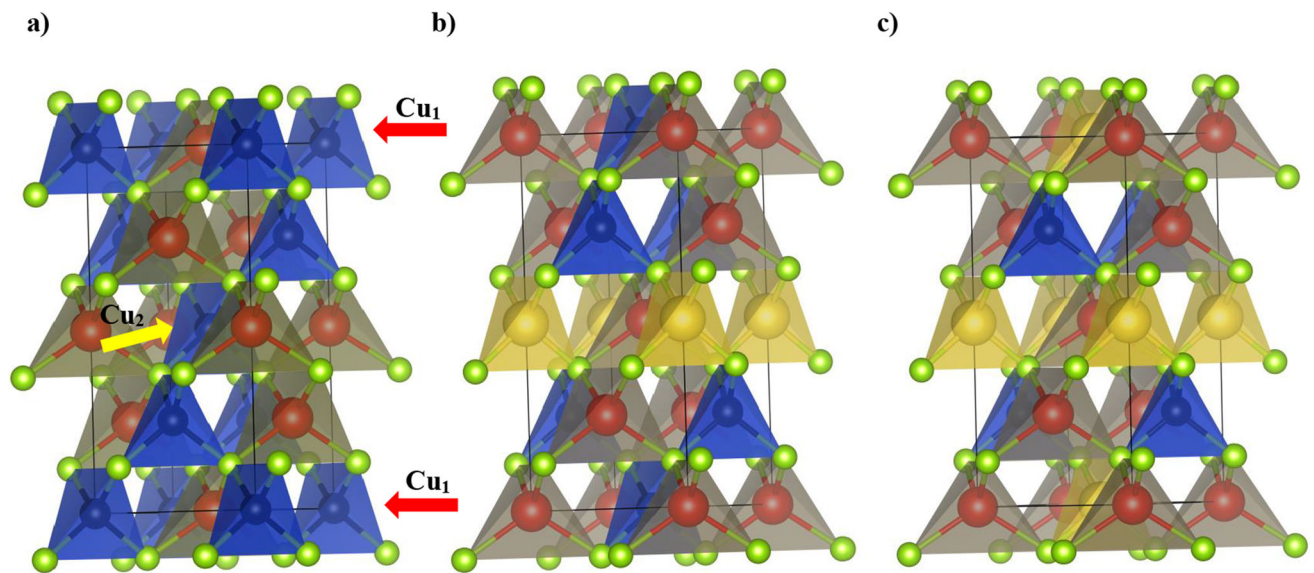
[b] e-mail: khenata_rabah@yahoo.fr (corresponding author)

Fig. 1 Crystal structures of $CuTlSe_2$ (**a**), $Cu_{0.75}Na_{0.25}TlSe_2$ (when Cu_1 is replaced) (**b**), and $Cu_{0.50}Na_{0.50}TlSe_2$ (when Cu_1 and Cu_2 are replaced) (**c**) Cu (black filled circle), Tl (red filled circle), Se (green filled circle), Na (yellow filled circle)

$CuTlSe_2$ compound have been reported. In this context, we propose a strategy to boost the thermoelectric efficiency of $CuTlSe_2$ by alloying it with the Na atom, which may enhance the Seebeck coefficient (S) and probably reduce the thermal conductivity (k), i.e., increase the ZT value, which quantifies the thermoelectric performance.

2 Crystal structure and computational details

The $CuTlSe_2$ compound adopts the chalcopyrite crystal structure, which is a tetragonal system with space group *I-42d* (no. 122) [22]. In this structure, the Cu, Tl, and Se atoms are located the *4a* (0, 0, 0), *4b* (0, 0, 1/2), and *8d* (0.23, 1/4, 1/8) Wyckoff positions, respectively. To model the crystalline structure of the $Cu_{0.75}Na_{0.25}TlSe_2$/$Cu_{0.50}Na_{0.50}TlSe_2$ compounds, we substituted one/two Cu atoms in the $CuTlSe_2$ ($1 \times 1 \times 2$) supercell with one/two Na atoms as shown in Fig. 1, panels b and c. The full potential linearized augmented plane wave (FP-LAPW) approach [23, 24] as incorporated in the WIEN2k package [25] was used to carry out all ab initio calculations. The exchange–correlation interactions were modeled using the Wu and Cohen [26] generalized gradient approximation GGA-WC functional to determine the optimized structural parameters, including the lattice parameters and atomic position coordinates, and the Tran and Blaha [27] modified Becke–Johnson TB-mBJ potential to calculate the electronic structure. Note that the TB-mBJ potential was specially developed to produce a bandgap value closer to the experimental counterpart than that provided by the standard GGA [28, 29]. There are some convergence parameters that should be set carefully for precise calculation, namely $R_{MT}^{min} K_{max}$, where K_{max} is the largest wave vector and R_{MT}^{min} is the smallest muffin-tin sphere radius, angular momentum cut-off (ℓ_{max}), muffin-tin radii (R_{MT}), and number of the k-points in the irreducible Brillouin zone (IBZ). For good convergence of the performed calculations, we choose $R_{MT}^{min} K_{max} = 8$, R_{MT} (Cu) = 2.1 a.u., R_{MT} (Tl) = 2.36 a.u., R_{MT} (Se) = 1.9 a.u., R_{MT} (Na) = 2.1 a.u., $\ell_{max} = 10$, and 99 k-points in IBZ. The crystal structure was optimized by minimizing the forces acting on each constituent atom with convergence criteria set to 10^{-4} Ryd/Bohr. The total energy convergence criterion was set to 10^{-4} Ryd. The BoltzTrap code [30], which is an implementation of the Boltzmann transport theory with the rigid-band model and constant-scattering time approximation (CSTA), was used to calculate the thermoelectric parameters. For precise calculation of the thermoelectric parameters, a dense mesh of 6083 k-points in the IBZ was used.

3 Results and discussion

3.1 Structural properties

The lattice parameters (a and c) along with the bulk modulus B, and its pressure derivative B' for the $Cu_{1-x}Na_xTlSe_2$ ($x = 0.00$, 0.25, 0.50) compounds, calculated by fitting total energy versus unit cell volume to Murnaghan equation of state [31], are collected in Table 1 together with the available experimental counterparts. The obtained lattice parameters of $CuTlSe_2$ agree well with the available experimental results [32]. Note that there are no available data for the structural parameters for the $Cu_{1-x}Na_xTlSe_2$ ($x =$

Table 1 The calculated lattice parameters (a and c, in Å), bulk modulus (B, in GPa), bulk modulus pressure derivative (B'), formation energy (E_f, (in kJ/mol), bandgap (E_g, in eV), and electron/hole effective mass ($m_\mathrm{e}/m_\mathrm{h}$, in m_0 "the rest mass of an electron" unit)

	a	c	B	B'	E_f	E_g	m_e	m_h
$CuTlSe_2$ present work	5.829	11.90	56.95	5.04	-313.58	0	0.07	0.41
Expt	5.83 [16]	11.60 [16]			-294.4 [17]			
$Cu_{0.75}Na_{0.25}TlSe_2$	5.851	12.343	48.87	5.13	-284.63	0.175	0.06	0.67
$Cu_{0.50}Na_{0.50}TlSe_2$	5.925	12.100	41.29	5.21	-256.62	0.352	0.05	0.85

0.25, 0.50) compounds in the literature. Table 1 shows that both a and c increase with increasing composition of the Na atom (x) in the $Cu_{1-x}Na_xTlSe_2$ alloy, while the bulk modulus decreases with increasing x.

Besides, the formation energy E_f per atom is calculated in order to examine the thermodynamic stability of the $Cu_{1-x}Na_xTlSe_2$ alloys using the following relations:

$$E_\mathrm{f}(Cu_{1-x}Na_xTlSe_2) = 1/N(E_\mathrm{T}(Cu_{1-x}Na_xTlSe_2) - [(1-x)E_{Cu} + xE_{Na} + E_{Tl} + 2E_{Se}]) \qquad (1)$$

Here, E_T is the total energy of the $Cu_{1-x}Na_xTlSe_2$ alloys, N is the number of atoms, E_{Cu}, E_{Tl}, E_{Na} and E_{Se} are the energies of Cu (cubic, Pm3m), Tl (cubic, Fm3m), Na (cubic, I43m), and Se (cubic, Pm3m) atoms, respectively, in their solid state. Calculated formation energies for all considered $Cu_{1-x}Na_xTlSe_2$ alloys are negative as can be seen from Table 1, indicating their thermodynamic stability. Note that the calculated E_f value for $CuTlSe_2$ compound is in good agreement with that estimated by Kumar and Sastry [33].

3.2 Electronic properties

Both GGA-WC and TB-mBJ were used to calculate the energy band dispersions (Fig. 2) of the $Cu_{1-x}Na_xTlSe_2$ compounds. The GGA-WC band structure reveals that $CuTlSe_2$ is of metallic character, while the TB-mBJ one with including spin–orbit coupling (SOC) (Fig. 2) shows semi-metallic character, which is consistent with the work of Ruan et al. [11]. However, both $Cu_{0.75}Na_{0.25}TlSe_2$ and $Cu_{0.50}Na_{0.50}TlSe_2$ alloys are found to be semiconductors with direct narrow band gap at (Γ–Γ) of about 0.17 eV (0.06 eV) and 0.35 eV (0.15 eV), respectively, using TB-mBJ (GGA-WC). Note that the inclusion of SOC does not affect the bandgap values of the considered alloys. The transition from semi-metallic character to semiconductive nature after Na-doping results from the shift of the minimum conduction band (MCB) toward higher energy. From Table 1, it can be seen that the bandgap value increases with increasing Na composition in the $Cu_{1-x}Na_xTlSe_2$ alloys; the bandgap value increased of about 0.177 eV when x increased from 0.25 to 0.50. This increase can mainly be attributed to the change in the valence states and the difference in electronegativity [34] between Cu (1.9) and Na (0.93) atoms.

We calculated the electron effective mass ($m_\mathrm{e}*$) at the MCB and the hole effective mass ($m_\mathrm{h}*$) at the maximum valence band (MVB) for $Cu_{1-x}Na_xTlSe_2$ alloys via the following equation:

$$m^* = \hbar^2\left(\frac{\mathrm{d}^2 E}{\mathrm{d}k^2}\right)^{-1} \qquad (2)$$

where the continuous function $E(k)$ was obtained by fitting the energies E at the band edge positions k to the parabolic function and $\hbar$ is the reduced Planck constant [35, 36].

It appears from Table 1 that the effective mass of the electron at MCB is smaller than that of the hole at MVB for the $CuTlSe_2$ alloys. This may be attributed to the fact that the minimum conduction band is more dispersive than the maximum valence band. The hole effective mass increases with increasing Na composition in the $Cu_{1-x}Na_xTlSe_2$ alloys, while the electron effective mass is slightly changed, which is due to the fact that the slopes of the MCB remain somewhat unchanged (see Fig. 2).

To understand the electronic structure of $Cu_{1-x}Na_xTlSe_2$ ($x = 0.00, 0.25$ and 0.50) materials, it is essential to calculate the density of states (DOS) diagram. Figure 3 depicts the calculated DOS spectra using the TB-mBJ potential. It is clear from Fig. 3 that the valence band close to the Fermi level of the $CuTlSe_2$ material is mainly originated from the Cu-3d states hybridized with the Se-4p and Tl-6p states, and the conduction band close to the Fermi level is dominated by the Tl-6s states hybridized with the Se-4p and Cu-3d states. When the copper is substituted by the sodium, we remark the apparition of new states in the MVB due to the '2p' states of Na, and the conduction states in the energy range 0–1.3 eV, formed mainly by Tl-6s and Se-4p states, are pushed toward higher energy. Consequently, $Cu_{0.75}Na_{0.25}TlSe_2$ and $Cu_{0.50}Na_{0.50}TlSe_2$ have semiconductor character with a bandgap energy of about 0.17 eV and 0.35 eV, respectively.

For a better understanding of charge distribution in the studied materials, the electron charge distribution map was calculated in the (112) plane, which involves all constituent atoms. Figure 4a shows that the charge in $CuTlSe_2$ is shared between the cations (Cu, Tl) and the anion atom Se, confirming the formation of a covalent bond between them. When the Na substitutes the Cu atom, a high charge accumulation in the vicinity of the anion occurs, which is caused by the electron transfer from the Na atom to the Se atom (Fig. 4b, c), and since there is a high electronegativity difference between Na and Se, which is about 1.62, a Na–Se ionic

Fig. 2 Calculated band structure
of CuTlSe$_2$ (**a**),
Cu$_{0.75}$Na$_{0.25}$TlSe$_2$ (**b**), and
Cu$_{0.50}$Na$_{0.50}$TlSe$_2$ (**c**)
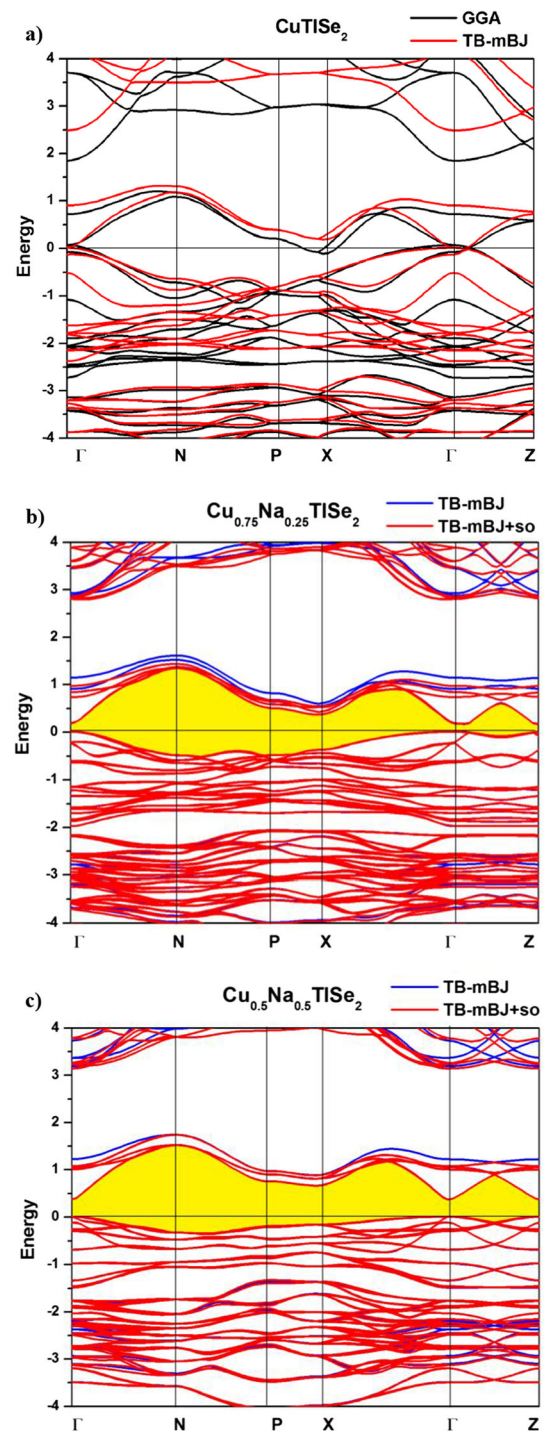
bond is formed. This new Na–Se ionic bond is responsible for the metal–semiconductor transition in the Cu$_{1-x}$Na$_x$TlSe$_2$ alloy. By increasing the concentration of Na, stronger ionic bonds are formed (Fig. 4c) and hence, the bandgap value is increased.

3.3 Thermoelectric coefficients

Knowledge of material's thermoelectric properties is essential for device manufacture. We computed temperature-dependent thermoelectric transport coefficients of Cu$_{1-x}$Na$_x$TlSe$_2$ alloys using the semi-classical Boltzmann transport theory. Figure 5 illustrates the chemical potential dependence of the Seebeck coefficient, electrical conductivity, thermal conductivity, and power factor at absolute temperatures of 300 K, 600 K, and 800 K for Cu$_{1-x}$Na$_x$TlSe$_2$ compounds.

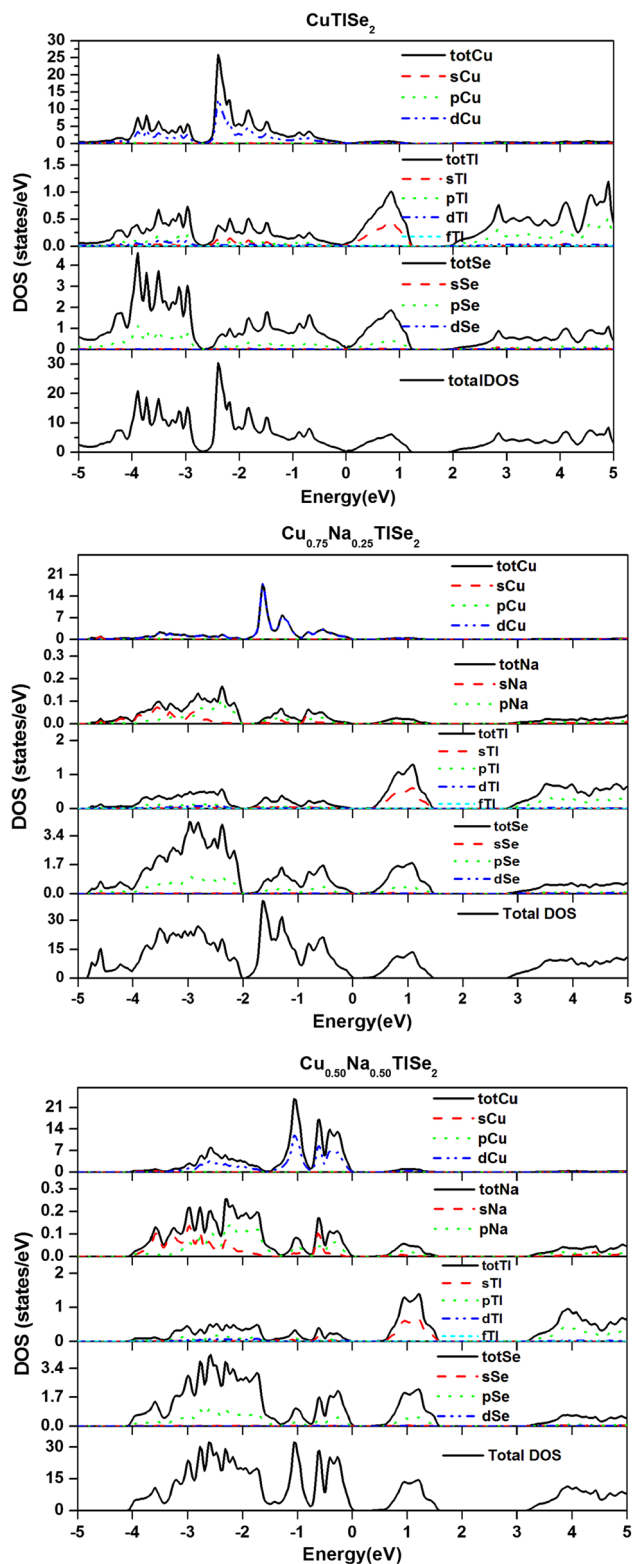**Fig. 3** Density of states of $Cu_{1-x}Na_xTlSe_2$ ($x = 0.00, 0.25$, and 0.50) alloys

Figure 5a shows that the Seebeck coefficient value at Fermi level is $-19.27\,\mu V/K$ for $CuTlS_2$, $148.84\,\mu V/K$ for $Cu_{0.75}Na_{0.25}TlSe_2$, and $180.77\,\mu V/K$ for $Cu_{0.50}Na_{0.50}TlSe_2$. Knowing that the Seebeck coefficient value for *n*-doped materials is negative and positive for *p*-doped materials, we conclude that $CuTlSe_2$ is an *n*-type conductivity material with electrons as the majority charge carriers, whereas $Cu_{0.75}Na_{0.25}TlSe_2$ and $Cu_{0.5}Na_{0.5}TlSe_2$ alloys are of *p*-type conductivity materials proving that the majority charge carriers are holes. Consequently, alloying $CuTlSe_2$ with Na leads to a transition from *n*-type to *p*-type conductivity, which can be elucidated

Fig. 4 Contour plots of the charge density distribution in color scale, $\Delta n(r)$: nuances of rendering resolution of the charge density, for $Cu_{1-x}Na_xTlSe_2$ ($x = 0.00$, 0.25, and 0.50) alloys. Red color (+ 0.0) represents no charge, while pink color (+ 1.0) represents the maximum charge accumulation site

Scale: $\Delta n(r)$	
■	+0.0001
□	+0.2001
■	+0.4001
■	+0.6000
■	+0.8000
■	+1.0000
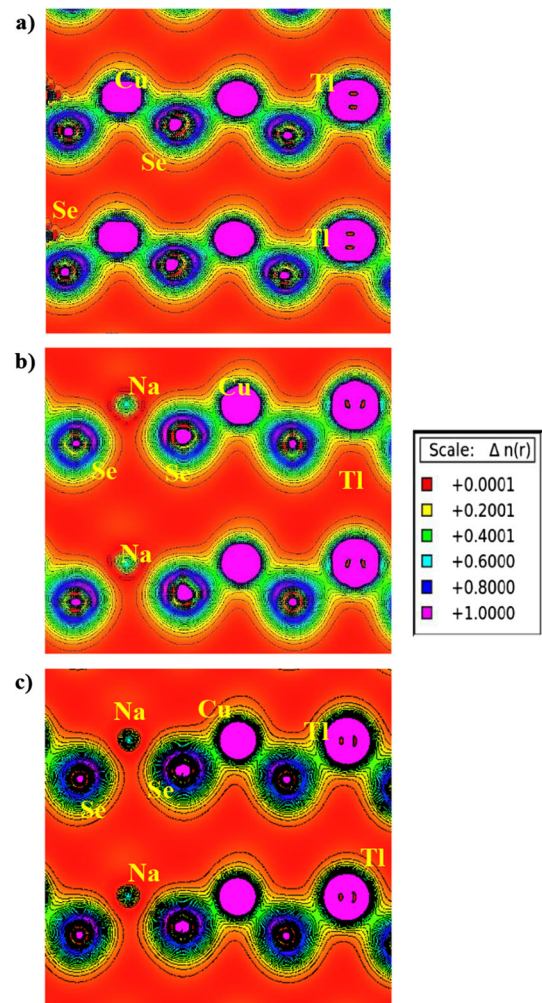
by the shift of the Fermi level into the edge of the valence band for $Cu_{1-x}Na_xTlSe_2$ alloys (Fig. 2). Knowing that the Seebeck coefficient is proportional with the effective mass, $S = \frac{8\pi k_B T}{3eh} m * (\frac{\pi}{3n})^{2/3}$ [37]; the increase in S with increasing Na composition can be attributed to the flatness of the valence band maximum (VBM) in the case of $Cu_{0.50}Na_{0.50}TlSe_2$ alloy, suggesting a higher hole effective masse (m_h*) (Table 1). Moreover, this increase in the S value can also be attributed to the increase in DOS near the Fermi level with increasing Na atom composition (see Fig. 3). Besides, it is also observed that the Seebeck coefficient value decreases with increasing temperature.

Panels of Figure 5d–f show that the electrical conductivity decreases with increasing Na composition in $Cu_{1-x}Na_xTlSe_2$ and is less affected by temperature. This behavior can be explained by the increase in the ionic character with the increase in the Na concentration due to the increase in the ionic bonds Na–Se. The electronic thermal conductivity (κ_e) is related to the electrical conductivity (σ) through Wiedemann–Franz relation $\kappa_e = L\sigma T$, where L is the Lorenz number; thus, κ_e will vary with temperature (T) and Na composition as σ. Low thermal conductivity is required for efficient TE materials. Figure 5j–l represents the variation of the power factor (PF) with the chemical potential at the absolute temperatures of 300 K, 600 K and 800 K for the $Cu_{1-x}Na_xTlSe_2$ alloys. It appears from Fig. 5j–l that $CuTlSe_2$ has a maximum value of PF for *n*-type, whereas both alloys $Cu_{1-x}Na_xTlSe_2$ ($x = 0.25, 0.50$) have higher peak for *p*-type at room temperature. Similarly, PF has a maximum for *n*-type in the case of $CuTlSe_2$ and $Cu_{0.75}Na_{0.25}TlSe_2$ at high temperature.

3.3.1 Figure of merit

As mentioned in the introduction, to determine the figure of merit ZT, one needs to estimate the total thermal conductivity ($\kappa = \kappa_e + \kappa_l$), and since the BoltzTrap code yields only the electronic thermal conductivity (κ_e), we calculated the thermal lattice conductivity (κ_l) using the Slack model formula [38]:

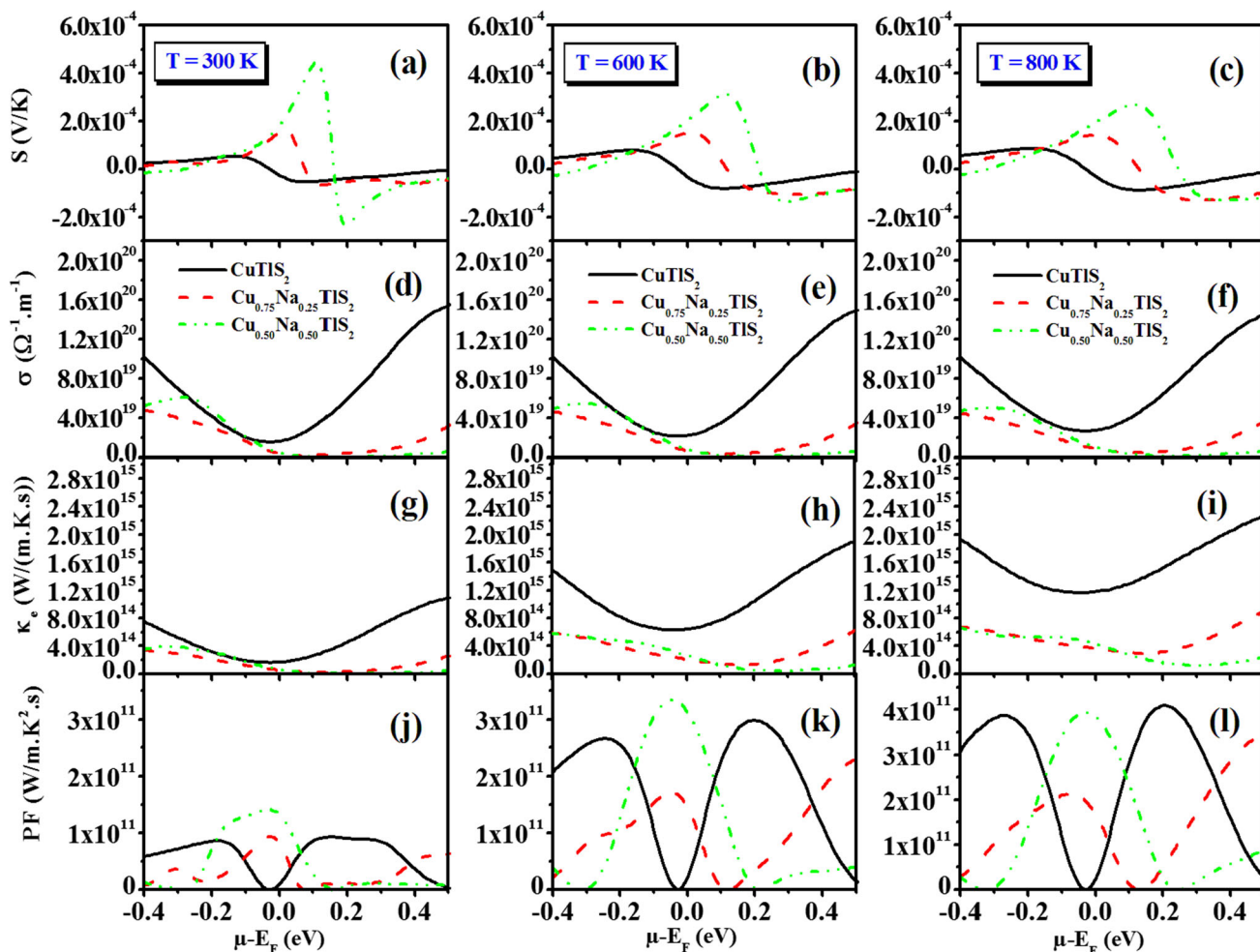$$\kappa_l = A \cdot \frac{\overline{M}\theta_D^3\delta}{\gamma^2 T n^{2/3}} \tag{3}$$

Fig. 5 Seebeck coefficient, electronic conductivity, electronic thermal conductivity, and power factor of $Cu_{1-x}Na_xTlSe_2$ ($x = 0.00, 0.25$, and 0.50) alloys at absolute temperatures of 300 K, 600 K, and 800 K

where $\overline{M}$ is the average atomic mass of all constituent atoms, A is a constant determined as [39]: $A = \frac{2.43.10^{-8}}{1 - \frac{0.514}{\gamma} + \frac{0.228}{\gamma^2}}$, δ is the average atomic volume to the power of (1/3), T is the absolute temperature, n is the number of atoms in primitive cell, γ is the Grüneisen parameter, and θ_D is the Debye temperature. γ and θ_D can be estimated through the quasi-harmonic Debye model integrated in the GIBBS2 program [40]. The estimated lattice conductivity for $Cu_{1-x}Na_xTlSe_2$ alloys is illustrated in Fig. 6. On the other hand, the relaxation time τ is estimated based on deformation potential theory [41] in which the acoustic phonon modes coupling with the free carrier is considered. According to DP theory, τ is given by:

$$\tau = \frac{2\sqrt{2\pi}\hbar^4 C_{ii}}{3(m^* k_B T)^{3/2} E^2} \tag{4}$$

where $\hbar$, m^*, C_{ii}, T, k_B, and E are, respectively, the reduced Planck constant, effective mass [hole mass (m_h^*) for p-type or electron mass (m_e^*) for n-type], elastic constants, absolute temperature, Boltzmann constant, and deformation potential constant of the MCB for electron or MVB for hole. The obtained electron/hole relaxation time (τ) for $Cu_{1-x}Na_xTlSe_2$ alloys is presented in Fig. 7. It is evident that the temperature dependence of τ is similar in the three alloys (see Fig. 7); it decreases when the temperature increases. This behavior can be explained by the fact that the thermal speed of electrons increases when the temperature increases; thus, the collisions between electrons become more important, and then, the amplitude of vibration of the atoms around their equilibrium positions increases. The calculated figure of merit ZT considering both electronic and lattice thermal conductivities for $Cu_{1-x}Na_xTlSe_2$ alloys at the absolute temperatures 300 K, 600 K and, 800 K is presented in Fig. 8. At room temperature, the maximum ZT is about 0.09 and 0.10 for $CuTlSe_2$ of p-type and n-type. When part of the Cu atoms is replaced by Na atoms, the ZT value increases to reach a maximum of about 0.46 and 0.87 for p-type $Cu_{0.75}Na_{0.25}TlSe_2$ and n-type $Cu_{0.50}Na_{0.50}TlSe_2$, respectively. The aforementioned ZT maximums, i.e., 0.46 for p-type $Cu_{0.75}Na_{0.25}TlSe_2$ and 0.87 for n-type $Cu_{0.50}Na_{0.50}TlSe_2$, correspond to

Fig. 6 The estimated lattice
conductivity κ_1 for
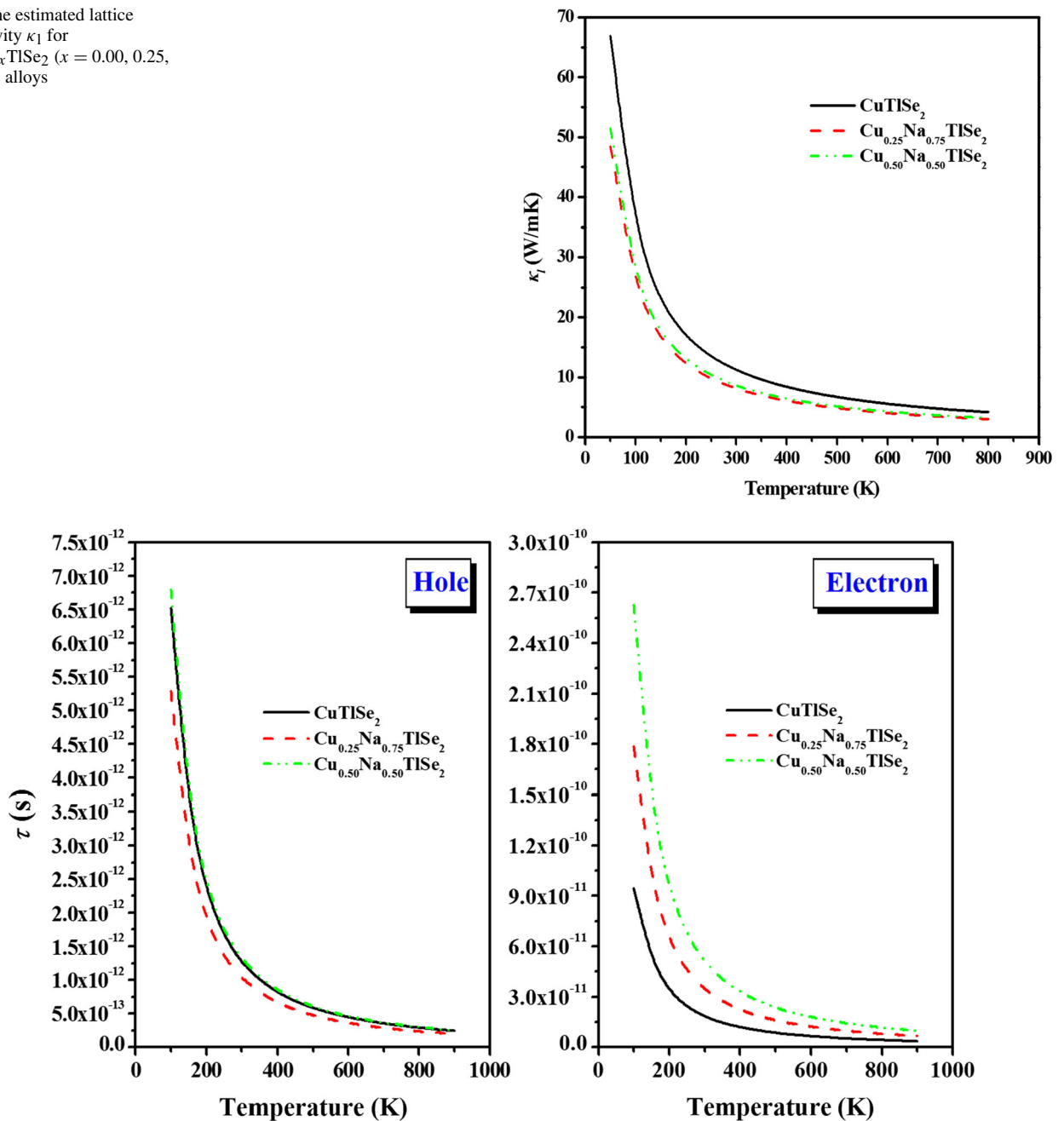$Cu_{1-x}Na_xTlSe_2$ ($x = 0.00, 0.25,$
and 0.50) alloys

Fig. 7 The calculated hole/electron relaxation time for $Cu_{1-x}Na_xTlSe_2$ ($x = 0.00, 0.25,$ and 0.50) alloys

carrier concentrations of about 1.7×10^{20} cm^{-3} and 2×10^{20} cm^{-3}, respectively. By increasing the temperature, the ZT$_{max}$ values gradually decrease and the corresponding peaks move toward the low chemical potential region.

4 Conclusion

The equilibrium structural parameters, electronic structure, and thermoelectric parameter properties of the $Cu_{1-x}Na_xTlSe_2$ ($x = 0.00, 0.25,$ and 0.50) were explored using first-principles calculations based on density functional theory. Calculated TB-mBJ band structure shows that $CuTlSe_2$ is a semimetal material and undergoes a metal–semiconductor transition when Cu is replaced by Na atoms. As a result, a direct band gap is observed for $Cu_{1-x}Na_xTlSe_2$ ($x = 0.25$ and 0.50) alloys. Such band gap energy was found to increase with increasing Na concentration, from 0.17 eV for $Cu_{0.75}Na_{0.25}TlSe_2$ to 0.35 eV for $Cu_{0.50}Na_{0.50}TlSe_2$. This behavior is caused by the formation of new Na–Se bond $Cu_{1-x}Na_xTlSe_2$ alloys ($x = 0.25$ and 0.50). Moreover, the effect of alloying $CuTlSe_2$
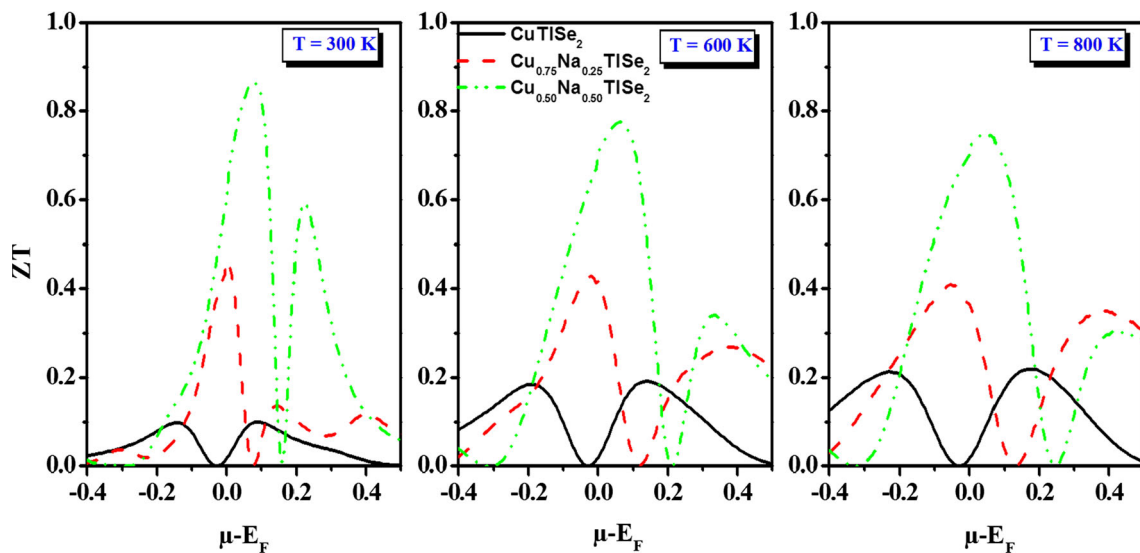
Fig. 8 Electronic figure of merit at absolute temperatures of 300 K, 600 K, and 800 K for $Cu_{1-x}Na_xTlSe_2$ ($x = 0.00$, 0.25, and 0.50) alloys

with Na on thermoelectric coefficients was studied in detail. The results show that $Cu_{0.50}Na_{0.50}TlSe_2$ marked the highest Seebeck coefficient and power factor, which leads to the highest ZT of about 0.87 at room temperature. Consequently, the Na substitution enhances the thermoelectric properties of $CuTlSe_2$, making it a promising compound for power generation.

Data availability statement No data are associated in the manuscript.

Declarations

Conflict of interest The authors declare that they have no known competing financial interests or personal relationships that could have appeared to influence the work reported in this paper.

References

1. H.J. Goldsmid, R.W. Douglas, The use of semiconductors in thermoelectric. Br. J. Appl. Phys. **5**(111), 458 (1954)
2. J.-A. Dolyniuk, B. Owens-Baird, J. Wang, J. Zaikina, K. Kovnir, Clathrate thermoelectrics. Mater. Sci. Eng. R. Rep. **108**, 1–46 (2016)
3. M. Rull-Bravo, A. Moure, J.F. Fernández, M. Martín-González, Skutterudites as thermoelectric materials: revisited. RSC Adv. **5**, 41653–41667 (2015)
4. G. Rogl, A. Grytsiv, P. Rogl, E. Bauer, M. Kerber, M. Zehetbauer, S. Puchegger, Multifilled nanocrystalline p-type didymium–Skutterudites with ZT> 1.2. Intermetallics **18**(112), 2435–2444 (2010)
5. S. Kauzlarich, S. Brown, G. Snyderk, Zintl phases for thermoelectric devices. Dalton Trans. **121**, 2099–2107 (2007)
6. A. Banik, U.S. Shenoy, S. Anand, U.V. Waghmare, K. Biswas, Mg alloying in SnTe facilitates valence band convergence and optimizes thermoelectric properties. Chem. Mater. **27**(12), 581–587 (2015)
7. Q. Zhang, B. Liao, Y. Lan, K. Lukas, W. Liu, K. Esfarjani, C. Opeil, D. Broido, G. Chen, Z. Ren, High thermoelectric performance by resonant dopant indium in nanostructured SnTe. Proc. Natl. Acad. Sci. U.S.A. **110**(133), 13261–13266 (2013)
8. P. Carruthers, Theory of thermal conductivity of solids at low temperatures. Rev. Mod. Phys. **33**(11), 92–138 (1961)
9. D.E.S. Mohammed, T. Seddik, M. Batouche, O. Merabiha, A. Zanoun, Improvement of electronic and thermoelectric properties of the metallic LaS by sodium substitution: From first-principles calculations. J. Appl. Phys. **123**(19), 095106 (2018)
10. R. Venkatasubramanian, E. Siivola, T. Colpitts, B. O'Quinn, Thin-film thermoelectric devices with high room-temperature figures of merit. Nature **143**, 597–602 (2001)
11. J. Ruan, S. Jian, D. Zhang, H. Yao, H. Zhang, S. Zhang, D. Xing, Ideal Weyl semimetals in the chalcopyrites $CuTlSe_2$, $AgTlTe_2$, $AuTlTe_2$, and $ZnPbAs_2$. Phys. Rev. Lett. **116**(122), 226801 (2016)
12. V.K. Gudelli, V. Kanchana, G. Vaitheeswaran, A. Svane, N.E. Christensen, Thermoelectric properties of chalcopyrite type $CuGaTe_2$ and chalcostibite $CuSbS_2$. J. Appl. Phys. **114**, 1223707 (2013)
13. T. Plirdpring, K. Kurosaki, A. Kosuga, T. Day, S. Firdosy, V. Ravi, G.J. Snyder, A. Harnwunggmoung, T. Sugahara, Y. Ohishi, H. Muta, S. Yamanaka, Chalcopyrite $CuGaTe_2$: a high-efficiency bulk thermoelectric material. Adv. Mater. **24**(127), 3622–3626 (2012)

14. R. Liu, L. Xi, H. Liu, X. Shi, W. Zhang, L. Chen, Ternary compound $CuInTe_2$: a promising thermoelectric material with diamond-like structure. Chem. Commun. **48**(132), 3818–3820 (2012)

15. D. Berthebaud, O.I. Lebedev, A. Maignan, Thermoelectric properties of n-type cobalt doped chalcopyrite $Cu_{1-x}Co_xFeS_2$ and p-type eskebornite $CuFeSe_2$. J. Materiomics **1**(11), 68–74 (2015)

16. J. Simon, G. Guelou, B. Srinivasan, D. Mori, A. Maignan, Exploring the thermoelectric behavior of spark plasma sintered $Fe_{7-x}Co_xS_8$ compounds. J. Alloys **819**(1152999), 1–10 (2020)

17. J. Navratil, J. Kašparová, T. Plecháče, L. Beneš, Z. Olmrová-Zmrhalová, V. Kucek, Č Drašar, Thermoelectric and transport properties of n-type palladium-doped chalcopyrite $Cu_{1-x}Pd_xFeS_2$ compounds. J. Electron. Mater. **48**, 1795–1804 (2019)

18. Z. Xia, G. Wang, X. Zhou, W. Wen, Substitution defect enhancing thermoelectric properties in $CuInTe_2$. Mater. Res. Bull. **101**, 184–189 (2018)

19. F. Ahmed, N. Tsujii, T. Mori, Thermoelectric properties of $CuGa_{1-x}Mn_xTe_2$: power factor enhancement by incorporation of magnetic ions. J. Mater. Chem. A **5**(116), 7545–7554 (2017)

20. P. Poudeu, J. D'Angelo, A. Downey, J. Short, T. Hogan, M. Kanatzidis, High thermoelectric figure of merit and nanostructuring in bulk *p*-type $Na_{1-x}Pb_mSb_yTe_{m+2}$. Angew. Chem. **45**(123), 3835–3839 (2006)

21. M. Moutassem, T. Seddik, D. Mohammed, M. Batouche, H. Khachai, R. Khenata, R. Ahmed, V. Srivastava, A. Bouhemadou, A. Kushwaha, S.B. Omran, Metal to semiconductor transition and figure of merit enhancement of Li_2CuAs compound by Na substitution. Bull. Mater. Sci. **45**(13), 1–10 (2022)

22. Y.J. Dong, Y.L. Gao, Density function theory of elastic and thermal properties for $CuTlSe_2$ crystal. Chalcogenide Lett. **13**(110), 515–520 (2016)

23. P. Hohenberg, W. Kohn, Inhomogeneous electron gas. Phys. Rev. **136**(13B), B864–B871 (1964)

24. W. Kohn, L. Sham, Self-consistent equations including exchange and correlation effects. Phys. Rev. **140**(14A), A1133–A1138 (1965)

25. P. Blaha, K. Schwar, G.K.H. Madsen, D. Kvasnicka, J. Luitz, R. Laskowski, F. Tran, L.D. Marks, *WIEN2k an augmented plane wave plus local orbitals program for calculating crystal properties* (Vienna University of Technology, Vienna, 2001)

26. Z. Wu, R. Cohen, More accurate generalized gradient approximation for solids. Phys. Rev. B **72**(123), 235116–235122 (2006)

27. F. Tran, P. Blaha, Band gaps of semiconductors and insulators with a semilocal exchange-correlation potential. Phys. Rev. Lett. **102**(122), 226401–226405 (2009)

28. J. Camargo-Martínez, R. Baquero, Performance of the modified Becke–Johnson potential for semiconductors. Phys. Rev. B **86**(119), 195106–195113 (2012)

29. D. Koller, F. Tran, P. Blaha, Improving the modified Becke–Johnson exchange potential. Phys. Rev. B **85**(115), 155109 (2012)

30. G. Madsen, D. Singh, BoltzTraP. A code for calculating band-structure dependent quantities. Comput. Phys. Commun. **175**(11), 67–71 (2006)

31. F. Birch, Elasticity and constitution of the Earth's interior. J. Geophys. Res. **57**(12), 227–286 (1952)

32. D. Singh, Electronic transport in old and new thermoelectric materials. Sci. Adv. Mater. **3**(14), 561–570 (2011)

33. V. Kumar, B. Sastry, Heat of formation of ternary chalcopyrite semiconductors. J. Phys. Chem. Solids **66**(11), 99–102 (2005)

34. A. Allred, Electronegativity values from thermochemical data. J. Inorg. Nucl. Chem. **17**(13–4), 215–221 (1961)

35. V. Vu, V.T.T. Vi, H.V. Phuc, A.I. Kartamyshev, N.N. Hieu, Oxygenation of Janus group III monochalcogenides: first-principles insights into GaInXO (X=S, Se, Te) monolayers. Phys. Rev. B **104**(111), 115410 (2021)

36. B. Rezini, T. Seddik, R. Mouacher, T. Vu, M. Batouche, O. Khyzhun, Strain effects on electronic, optical properties and carriers mobility of Cs_2SnI_6 vacancy-ordered double perovskite: a promising photovoltaic material. Int. J. Quantum Chem. **122**(121), e26977 (2022)

37. E.M. Levin, Charge carrier effective mass and concentration derived from combination of Seebeck coefficient and 125Te NMR measurements in complex tellurides. Phys. Rev. B **93**(124), 245202 (2016)

38. G. Slack, The thermal conductivity of nonmetallic crystals. Solid State Phys. **34**, 1–71 (1979)

39. C. Julian, Theory of heat conduction in rare-gas crystals. Phys. Rev. **137**(11A), A128–A137 (1965)

40. A. Otero-de-la-Roza, D. Abbasi-Pérez, V. Luaña, Gibbs2: a new version of the quasiharmonic model code. II. Models for solid-state thermodynamics, features and implementation. Comput. Phys. Commun. **182**(110), 2232–2248 (2011)

41. J. Shockley, W. Bardeen, Deformation potentials and mobilities in non-polar crystals. Phys. Rev. **80**(11), 72–80 (1950)